Inelastic electron tunnelling in saturated molecules with different functional groups: correlations and symmetry considerations from a computational study

2008 J. Phys.: Condens. Matter 20 374111

(http://iopscience.iop.org/0953-8984/20/37/374111)

J. Phys.: Condens. Matter **20** (2008) 374111 (11pp) doi:10.1088/0953-8984/20/37/374111

Inelastic electron tunnelling in saturated molecules with different functional groups: correlations and symmetry considerations from a computational study

Alessandro Troisi

Department of Chemistry and Centre of Scientific Computing, University of Warwick, Coventry CV4 7AL, UK

Received 31 January 2008, in final form 22 April 2008
Published 26 August 2008
Online at stacks.iop.org/JPhysCM/20/374111

Abstract

The inelastic electron tunnelling (IET) spectra of a series of molecules with the commonest functional groups are evaluated computationally. It is found that ether, secondary amine and thioether groups do not leave any characteristic signatures on the IET spectrum (in comparison with simple alkanes) and they cannot be used as 'tracers' for the tunnelling path of the electron. In contrast, carbonyl and ester groups modify the appearance of the IET spectrum considerably. The series of computations was also used to validate, for the case of saturated molecules, the propensity rules for IET spectroscopy proposed in the literature. It is found that totally symmetric vibrations give the largest contribution to the spectrum and that there is no correlation between IET and infrared or Raman absorption intensities.

1. Introduction

A molecular electric junction is constituted by a single molecule in contact with two electrodes. Understanding its behaviour when subjected to an applied external voltage is the fundamental problem studied by molecular electronics, a field now entering in its maturity [1, 2]. The realization of experimental measures on nanojunctions is by itself a major scientific achievement, made possible by the improved methodologies in nanofabrication, surface chemistry control and scanning probe techniques [3–7]. After the initial concerns about the reproducibility of these experiments, it is now possible to compare measures realized in different laboratories [8] and to provide a general theoretical description of the underlying physics, at least in the simplest cases [2]. At very low voltages, in the linear response regime and in the absence of resonance between the molecular levels and the Fermi level of the electrodes, the electrons cross the molecular junction by simple tunnelling which can be described efficiently using perturbation theory [9], scattering formalism [10], or the more general non-equilibrium Green's function approach [11–13]. Current theoretical research on simple electron tunnelling focuses mainly on several difficult computational aspects such as the accurate and balanced description of the electronic structure of the electrode/molecule interface and the proper calculation of the geometry in the junction [14–17].

However, a number of more complicated phenomena can take place in a molecular junction due to the interaction between the electronic and nuclear degrees of freedoms and the possibility of multiple electronic states (with different net charge) stable within a given voltage range. The phenomenology is determined by the relative magnitude of the characteristic timescales of the system. The energy difference between the Fermi level and the closest molecular level, know as the energy gap ΔE_G, determines the tunnelling traversal time $\hbar/\Delta E_G$. The quantity Γ, quantifying the strength of the molecule–lead interaction, determines the permanence time $\hbar/\Gamma$ of an electron on a molecule connected to the lead. Indicating with M the effective electron–phonon coupling strength, the condition for 'week' coupling limit can be expressed as $|M/\sqrt{\Delta E_G^2 + (\Gamma/2)^2}| \ll 1$ [18]. In the weak coupling limit, the electron–phonon coupling produces only a small effect on the total conductance and it can be treated as perturbation. In the same limit, it is possible to treat the conformational changes inside the molecule 'adiabatically' (in the Born–Oppenheimer approximation sense), i.e. as if the conductance is simply a function of the conformation

and it is not affected by molecular motions. The role of conformational changes produced by the electric field [19–21] or just thermal energy [22, 23] has been studied, in fact, in this limit. In the opposite limit of very strong electron–phonon coupling, it is the molecule–electrode coupling that can be treated as a 'small perturbation' and the electron proceeds from one electrode to the other by a sequence of hopping events involving the molecular states. Although one can see a clear analogy between these two limiting cases and the cases of tunnelling and hopping studied in the classical papers on molecular solids [24, 25], in the molecular junction case the intermediate situations between these extremes seem to be extremely frequent and particularly important for device applications. For example, using a mean field model, Galperin *et al* [26] were able to show that the switching and bistability observed in several experiments [27, 28] can be due to two different steady states in the junctions with different electronic population and equilibrium geometry. The situation is further complicated by the presence of strong electric fields and electronic correlation within the molecule and between the transferred electron and the image charges on the leads. A very comprehensive review of these issues has been published recently [18].

In this paper we will focus on probably the most important of the effects recorded in the weak coupling limit, the off-resonance inelastic electron tunnelling (IET). In the simplest possible case of low-temperature weakly-coupled molecular junctions, the tunnelling electron has a finite probability of exciting one of the molecular vibrations losing the corresponding energy $\hbar\omega$. The process can occur for applied biases larger than a threshold voltage $V = \hbar\omega/e$ beyond which the inelastic channel is opened. This threshold appears as a small increase in conductance and it is better visualized as a peak in the plot of the current second derivative $(\mathrm{d}I^2/\mathrm{d}^2V)$ versus V. The phenomenon is further illustrated in figure 1. It should be noticed that in this inelastic process there is no resonance between the electronic states on the molecule and the Fermi levels on the electrode. The cross section for this process is very small (few percent of the conductance is due to the inelastic channel) but nevertheless sufficient to retrieve information on the vibrations of the molecules in the junction. The process is coherent (sometimes it is called co-tunnelling) and it should not be confused with the *incoherent inelastic tunnelling* which involves resonance of the molecular and electrode electronic states and possibly a finite lifetimes of the tunnelling electron on the molecule in the junction. An extensive discussion of the different meanings of 'inelastic transport' in molecular junction was given in [29, 30].

The origin of IET spectroscopy dates back in the late 60s, since when it has been used to characterize 'macroscopic' conductive surfaces [31, 32]. The first measure on a single molecule was done by Stipe *et al* in a STM configuration [33], while the first measures on molecules of relevance to molecular electronics (i.e. in contact with both electrodes) were presented by Kushmerick, in a cross-junction configuration [34], and Wang in a nanopore set up [35]. IET in single molecule is very different from the process observed macroscopically. In the latter, the electrons impact the molecules essentially as free particles, their interaction with the molecule is largely dominated by a charge–dipole interaction, and only a fraction of the electrons actually interact with the molecules (the presence of the molecule has a small effect on the total conductance differently from the molecular junction case). For this reason the understanding of inelastic tunnelling in single molecules could not be build on these previous experiments and developed instead from the theoretical models used to interpret STM images and other single molecule conductance experiments.

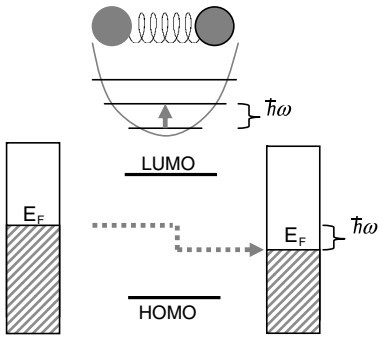

Figure 1. Illustration of the inelastic tunnelling process involved in IETS for an idealized system with only one vibrational degree of freedom at 0 K. The molecular levels HOMO and LUMO are not in resonance with the electrode Fermi levels at working biases. When the bias difference between the electrodes reaches the threshold $\hbar\omega/e$ the tunnelling electron can excite the vibration loosing an equivalent amount of energy. The extra inelastic channel opened at this bias is seen as a peak at $V = \hbar\omega/e$ in the plot of $\mathrm{d}^2I/\mathrm{d}V^2$ versus V.

The ability to predict and interpret the experimental IET spectra was immediately recognized as one of the most useful contributions that theory could give to the development of molecular electronics. IET spectroscopy (IETS) is, in fact, the only method universally applicable to characterize the junction (without need of additional measures beyond the electrical one), establishing the presence of the molecule, its chemical integrity and, possibly, also its environment and conformation.

The first theoretical models for off-resonance inelastic tunnelling were based on an extension of the Tersoff–Hamman formalism [36, 37] and focused on the explanation of STM-based measurement with simple semiempirical model Hamiltonian. A similar formalism with more sophisticated DFT computations were used for example by Persson and co-workers [37, 38]. Using a scattering formalism as a starting point we proposed a Herzberg-Teller like vibronic expansion of the electronic wavefunction to compute the inelastic conductance for the more general case of molecules strongly coupled to both electrodes [39]. The IET spectra simulated with this approach, in conjunction with standard quantum chemical calculations, were in remarkable agreement with the experimental data of Kushmerick *et al* [40] and allowed the interpretation of IETS spectra for hydrated junctions [41]. The same method was recently generalized by Toroker and Peskin [42] to include more efficiently the effect of the molecule–electrode vibrations. Luo and co-workers used a different formalism based on scattering theory [43] and they applied it to the study of the molecule–electrode [44] and intermolecular interactions as they can be

derived from IETS measures. The non-equilibrium Green's function formalism (NEGF) was the starting point of Paulsson *et al* [45, 46], who achieved also a very good comparison with the experiments in [40] and of Solomon *et al* [47] who applied their methodology on alkane thiolates. Unfortunately, the theoretical approaches differ not only for the adopted formalisms but also the quantum computational methods from which the relevant matrix elements are computed. Solomon *et al* adopted the density functional tight binding (DFTB) [48] methods that could offer great advantage if one has to optimize the geometry of large molecules on a surface [49]. Paulsson et al based their computation on the SIESTA Hamiltonian [50], similarly suited for large scale computations. For small molecules (see e.g. Teobaldi *et al* [51]) it is possible to perform very high level DFT computations including many atoms of the surface with plane waves basis set.

In a recent paper [52], the comparison between computed and experimental IET spectra of several compounds has led to an interesting additional application. Not only a satisfactory comparison may provide information on the structure of the junction but it can be also used to trace the tunnelling paths followed by the electron while traversing the junction. It can be easily verified that only vibrations that modulate the effective coupling between the electrodes are active in IETS so that, if a vibration localized on a portion of the molecule gives a strong IETS signal, one can conclude that the same portion of the molecule is involved in the tunnelling path of the electron. The concept of tunnelling paths has been used for long time [53, 54], especially in the context of electron transport in biology, but only through this type of measure it is possible to provide experimental proof of the passage of the electron from a particular portion of the molecule. In this paper we will explore the IETS signatures that could be given by a set of very common organic functional groups inserted within a saturated molecule (section 3.1). This work will be used as reference for the interpretation of future IETS measures and will guide the synthesis of molecules with the appropriate functional groups that can be used as 'tracer' for the passage of the electron.

The computations presented in this paper will also give the possibility of complementing previous discussions on symmetry propensity rules in IETS [55, 56], (focused on fully conjugated molecules) with new data on saturated molecules (section 3.2). Propensity rules are a particularly useful tool for the interpretation of spectra in the absence of a full theoretical simulation and it is also interesting to check if there is any correlation between the IETS computed intensities and the computed intensities for infrared (IR) and Raman spectroscopies. The results will be presented after an outline of the methodology.

2. Method

2.1. Intensity of IETS peaks

The total Hamiltonian of a molecular junction is partitioned in the three subspaces (left (L) and right (R) electrodes, and molecule (M)), where the independent components of the Hamiltonian are indicated as $H^{\mathrm{L}}, H^{\mathrm{R}}, H^{\mathrm{M}}$ and their interaction is $V^{\mathrm{LM}}, V^{\mathrm{RM}}$:

$$H = H^{\mathrm{L}} + H^{\mathrm{R}} + H^{\mathrm{M}} + V^{\mathrm{LM}} + V^{\mathrm{RM}}. \tag{1}$$

The zero-bias elastic conductance is [1, 2]:

$$g^{\mathrm{el}}(E_{\mathrm{F}}) = g_0 \,\mathrm{Tr}(\Gamma^{\mathrm{L}}(E_{\mathrm{F}})\mathbf{G}(E_{\mathrm{F}})\mathbf{\Gamma}^{\mathrm{R}}(E_{\mathrm{F}})\mathbf{G}(E_{\mathrm{F}})^{\dagger}) \tag{2}$$

E_{F} is the Fermi level, $g_0 = 2e^2/h$ is the quantum of conductance, $\mathbf{G}$ is the reduced Green's function matrix associated with the retarded Green's function operator $G(E) = (E - H + \mathrm{i}\varepsilon)^{-1}_{\varepsilon\to 0}$, and the matrices $\mathbf{\Gamma}^{\mathrm{L}}$ and $\mathbf{\Gamma}^{\mathrm{R}}$ are twice the imaginary part of the self-energy describing the molecular levels broadening due to the interaction with the metal. $\mathbf{\Gamma}^{\mathrm{L}}$ is defined as

$$\Gamma^{\mathrm{L}}_{ij}(E) = 2\pi \sum_l V^{LM^*}_{il} V^{\mathrm{LM}}_{lj} \delta(E - E_l) \tag{3}$$

where l runs over the one-electron eigenstates of H^{L}, and V^{LM}_{il} or V^{LM}_{lj} is the coupling between these and the orbitals on the molecule (indexes i and j). $\mathbf{\Gamma}^{\mathrm{R}}$ is defined analogously for the right electrodes and their explicit computation is described below.

$G(E)$ can be seen as a function of the dimensionless normal modes $\{Q_\alpha\}$ of the molecule and it is possible to define the matrices $\mathbf{G}^\alpha$ (α indicates a specific normal mode) as:

$$G^\alpha_{ij} = \frac{\sqrt{2}}{2}\left(\frac{\partial G_{ij}(E,\{Q_\alpha\})}{\partial Q_\alpha}\right)_{\{Q_\alpha\}=0}. \tag{4}$$

In [39] we proved that each vibrational mode α contributes to the IETS with a vibrational peak at energy $\hbar\omega_\alpha$ (and voltage $V = \hbar\omega_\alpha/e$), whose intensity is given by:

$$W_\alpha = g_0 \,\mathrm{Tr}(\mathbf{\Gamma}^{\mathrm{L}}(E_{\mathrm{F}})\mathbf{G}^\alpha(E_{\mathrm{F}})\mathbf{\Gamma}^{\mathrm{R}}(E_{\mathrm{F}})\mathbf{G}^\alpha(E_{\mathrm{F}})^{+}). \tag{5}$$

This equation is valid in the weak coupling limit discussed in the introduction, at low temperature ($k_B T \ll \hbar\omega_\alpha$), and was derived using a combination of scattering theory and perturbative treatment of the vibronic coupling. Equation (5) is particularly easy to implement and has the aesthetic appeal of being formally similar to equation (2). It is also particularly reassuring that a similar expression was derived by Gagliardi *et al* [57] using the NEGF formalism (in particular the Meir–Wingreen equation [58]) and introducing the Born approximation with the assumption that the inelastic conductance depends weakly on the injection energy [39]. Thanks to their work, equation (5) can be considered fully consistent with the more general NEGF approach when the appropriate low-temperature, low-voltage and large energy-gap limit are considered. Paulsson *et al* [45], compared the results of a full self-consistent Born approximation with the lowest order expansion in the electron–phonon coupling, finding an excellent agreement between the two. One particularly interesting feature of the approach leading to equation (5) is that it is particularly suitable for the computation of medium to large sized molecule and that the quality of the results increases with increasing the size of the

molecule because a smaller zero-bias conductance implies a reduced importance of the higher order effects neglected in equation (5).

The effect of the peak broadening (discussed theoretically in [59, 60]) is not included in the formalism and, as customary in computational spectroscopic studies, an arbitrary the broadening will be added to the computed spectrum. Also for convenience, the spectra will be plot as $(\mathrm{d}I^2/\mathrm{d}^2V)/(\mathrm{d}I/\mathrm{d}V)$ versus V, so that the areas under the IETS peaks are dimensionless values corresponding to the ratio $W_\alpha/g(E_\mathrm{F})$, which is the quantity reported in the tables.

2.2. Evaluation of the self-energy

The Green's function matrix in equations (2) and (5) is given by

$$\mathbf{G}(E) = (\mathbf{1}E - \mathbf{H} - \mathbf{\Sigma}^\mathrm{L} - \mathbf{\Sigma}^\mathrm{R})^{-1}, \tag{6}$$

where $\mathbf{H}$ represents the effective one-electron Hamiltonian of the molecule (the Konh–Fock matrix in this case) and $\mathbf{\Sigma}^{\mathrm{L/R}}$ are the self-energies associated with the left and right electrode. The imaginary component of the self-energy $\mathrm{Im}(\mathbf{\Sigma}^{\mathrm{L/R}}) = -\frac{1}{2}\mathbf{\Gamma}^{\mathrm{L/R}}$ was given in equation (3) and the real component $\mathrm{Re}(\mathbf{\Sigma}^{\mathrm{L/R}}) = \mathbf{\Lambda}^{\mathrm{L/R}}$ is given by:

$$\Lambda^\mathrm{L}_{ij}(E) = PP\sum_l \frac{V^*_{il}V_{lj}}{E - E_l}. \tag{7}$$

Representing the delocalized electrode orbitals $|l\rangle$ as linear combination of localized orbitals, e.g. $|l\rangle = \sum_k C_{lk}|k\rangle$, the product $\langle i|V|l\rangle\langle l|V|j\rangle$ can be written as $\sum_{k_1,k_2} C_{lk_1}C^*_{lk_2}\langle i|V|k_1\rangle\langle k_2|V|j\rangle$ and the spectral density becomes:

$$\begin{aligned}\Gamma^\mathrm{L}_{ij}(E) &= 2\pi\sum_{k_1,k_2}\langle i|V|k_1\rangle\langle k_2|V|j\rangle\sum_l C_{lk_1}C^*_{lk_2}\delta(E-E_l)\\ &= 2\pi\sum_{k_1,k_2}\langle i|V|k_1\rangle\rho_{k_1k_2}(E)\langle k_2|V|j\rangle\end{aligned} \tag{8}$$

where we have used the definition $\rho_{k_1k_2}(E) \equiv \sum_l C_{lk_1}C^*_{lk_2}\delta(E - E_l)$. Each term of equation (8) can be evaluated from quantum chemical computations. Since $|i\rangle$ and $|j\rangle$ are states localized on the molecule and $|k_1\rangle$, $|k_2\rangle$ are localized on the electrode, the summation extends only over relatively few pairs of localized orbitals. The matrix elements $\langle i|V|k_1\rangle$ can be obtained from cluster computations including few electrode atoms and the adsorbed molecule. The energy dependent density matrix is computed just once for a given surface. In the present case we derive it from a tight binding calculation of a large cluster of gold, exposing the (111) surface, as described in [61]. The explicit evaluation of $\mathbf{\Lambda}$ requires the same matrix elements:

$$\Lambda^\mathrm{L}_{ij}(E) = \sum_{k_1,k_2}\langle i|V|k_1\rangle R_{k_1k_2}(E)\langle k_2|V|j\rangle \tag{9}$$

and can be evaluated numerically using

$$\begin{aligned}R_{k_1k_2}(E) &= PP\sum_l \frac{C_{lk_1}C^*_{lk_2}}{E-E_l}\\ &= PP\int\sum_l \frac{C_{lk_1}C^*_{lk_2}}{E-E'}\delta(E'-E_l)\,\mathrm{d}E'\\ &= PP\int\frac{\rho_{k_1k_2}(E')}{E-E'}\,\mathrm{d}E'.\end{aligned} \tag{10}$$

We considered a set of linear molecules with thiol terminations at both ends, and oriented in such a way that the main axis of the molecule is perpendicular to the two electrodes. We assumed that the terminal S atoms are in a fcc adsorption site, and that the S–Au distance is 2.85 Å (this value derives from a geometry optimization performed in [61]). The Fermi energy was set to −0.12 Hartree (equivalent to −3.26 eV or −26 340 cm^{-1}) and no computations at finite bias were performed. The matrix elements $\langle i|V|k_1\rangle$ appearing in equations (8) and (9) are computed from a cluster containing 3 gold atoms of one electrode and the molecule (the right electrode is neglected when the self-energy of the left electrode is evaluated and vice versa). The LANL2MB basis set/pseudo potential is used for the gold atoms and the 6-31G* basis set is used for the other atoms. The hybrid DFT functional B3LYP was used to compute the effective one-electron Hamiltonian.

2.3. Computation of the normal modes and G^α

The normal modes needed for the computation of the IET spectra are computed for the isolated molecule which is optimized in the absence of the electrode. We are in fact interested in the IET response of functional groups distant from the electrode (see section 3.1) whose vibrations are only marginally affected by the molecule–electrode connection. The similarity between Raman spectra recorded in monolayer and in solution confirms that the isolated molecule vibrations are to an excellent degree of approximation transferable to the adsorbed molecule as verified also by the accurate IETS predictions in previous contributions. The optimized structure and normal modes are translated into the junction geometry for any given molecular orientation. Also these computations were performed at the B3LYP/6-31G* level (including the terminal hydrogen on the thiol group). This level of theory is a good compromise between speed and accuracy [62] and has the additional advantages of having been adopted by other authors [44], facilitating the comparison. Moreover, an extensive calibration work, done by comparing many experimental and theoretical IR and Raman spectra has lead to a proposed scaling factor for the computed frequencies [63] that will further help the comparison with the experiment.

The Green's function derivative of equation (4) needs to be computed for each mode, while the self-energy in $\mathbf{G}$, $\mathbf{G}^\alpha$ and W_α is computed once for each molecule. The intensity of the inelastic peaks is computed from equation (7). The numerical derivation was done using a displacement of 0.05 adimensional units. The component of the normal modes concerning the displacement of the hydrogen in the thiol group was disregarded. Normal modes have been classified according to the point group of the isolated molecules.

3. Results

3.1. Simulated IETS spectra

The set of six molecules included in this study are shown in figure 2 with the labels used to indicate them in the rest of the paper. **(1)** is a simple alkane with thiol groups connected to the terminal carbon atom 1 and 7 and it is used as a reference.

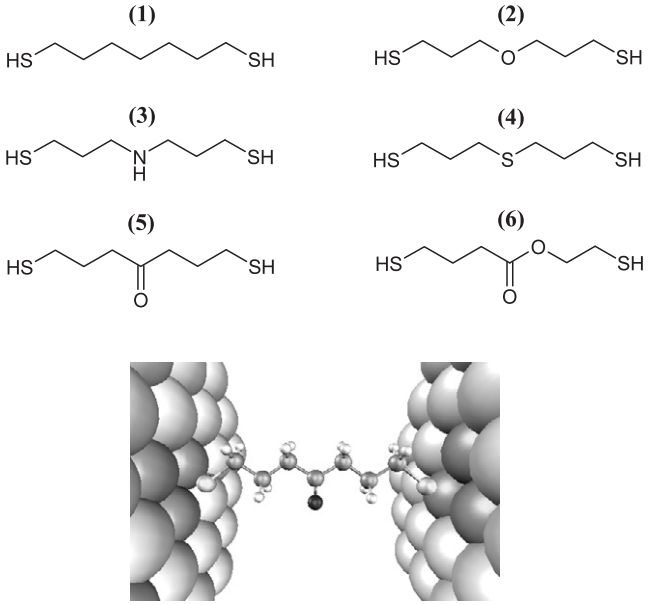

Figure 2. Top: Molecules studied in this paper with the labels used in the text. The hydrogen atoms of the thiol terminations are removed upon adsorption on gold. The distance between the thiol atom terminations is between 10.4 and 11.0 Å. Bottom: An illustration of the junction formed by molecule **(5)** between two gold surfaces.

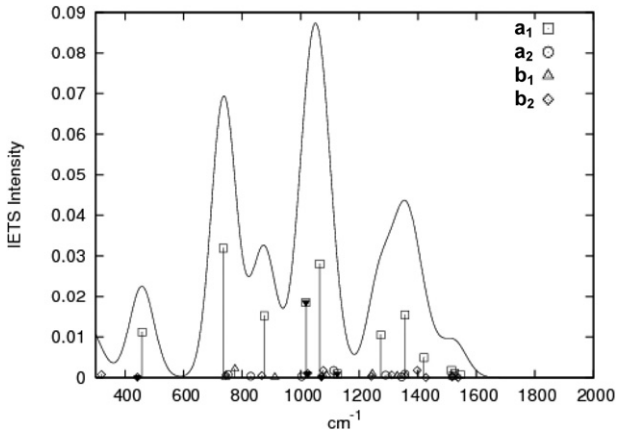

Figure 3. IETS computed spectrum for molecule **(1)**. The peaks are labelled according to their irreducible representations. The black triangles indicate the modes with the largest contribution of the central carbon.

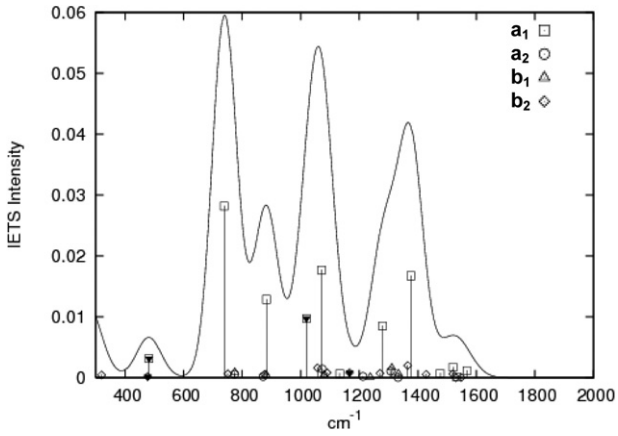

Figure 4. IETS computed spectrum for molecule **(2)**. The black triangles indicate the modes with the largest contribution of the functional group (see text).

In compounds **(2)**, **(3)**, **(4)**, **(5)** the central –CH_2– group is substituted with a ether, amine, thioether and carbonyl group respectively. In molecule **(6)** an ester function is introduced instead of carbon 5 and 6 of the original molecule. The length of the molecules is similar in all cases, the point group of the optimized molecules **(1)**, **(2)**, **(4)** and **(5)** is C_{2v}, while the point group of molecule **(3)** and **(6)** is C_s (but the symmetry plane is parallel to the electrodes in **(3)** and perpendicular to them in **(6)**). The set is selected primarily among the most common functional groups in organic chemistry, which can be inserted in an alkylic chain as potential 'tracer' for the passage of the electron. The characteristics vibrations of these modes are well characterized, tabled in textbooks on the spectroscopic identification of organic compounds [64], and it is interesting to verify here which functional groups give the most characteristic IETS signature. We considered functional groups 'embedded' in a saturated hydrocarbon chain because these highly non-polar moieties are the fundamental building blocks to realize ordered self-assembled monolayers on metal surfaces [65], one of the best starting point for accurate IETS measures. Moreover the spectrum of dithio-alkanes is well understood and the effect of the heterogroup can be more simply identified (both theoretically and experimentally) as a difference between the spectra of compounds **(2)**–**(6)** and compound **(1)**. A rather similar selection of model compounds was made by Claypool *et al* [66] to classify the appearance of the typical functional group of molecules adsorbed on graphite with STM. We finally note that the HOMO and LUMO position with respect to the Fermi lever is rather similar for all considered compounds so that we can exclude in the comparison of the spectra any effect due to resonance and quasi-resonance of the molecular level and the Fermi level at the considered biases. The HOMO energies range from −0.239 (compound **(6)**) to −0.224 Hartree (compound **(4)**) and the LUMO energy range from −0.022 (compound **(5)**) to 0.035 Hartree (compound **(1)**).

The spectra of the six compounds are presented graphically in the region 300–2000 cm^{-1} (figures 3–8) and in tables 1–6. To reduce the amount of information, the tables contain only the vibrations whose intensity is larger than 1/50 of the most intense peak. Only the vibrations with the largest IETS intensity in the spectral region of interest have been described qualitatively in the tables (description obtained by direct observation of the normal mode vectors). To simplify the discussion and the comparison with other works we did not include any scaling factor in the tabled frequencies and the plotted spectra, but we mention here that the recommended scaling factor for this level of theory is 0.961 [63]. The discussion of the spectra will focus on the window 300–2000 cm^{-1}. At lower energy the experimental spectrum is dominated by the so-called zero-bias feature (ZBF) [34], a large featureless peak probably due

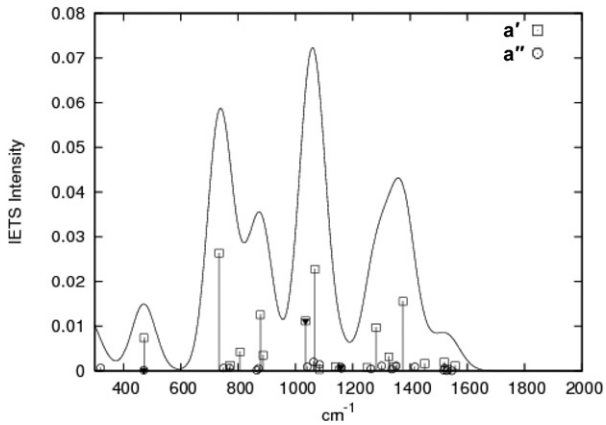

Figure 5. IETS computed spectrum for molecule (**3**).

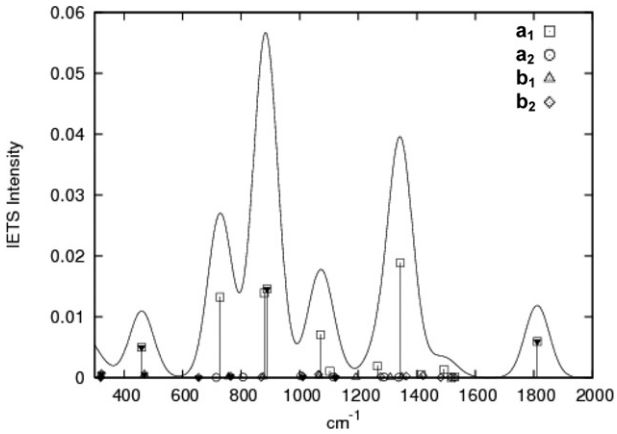

Figure 7. IETS computed spectrum for molecule (**5**).

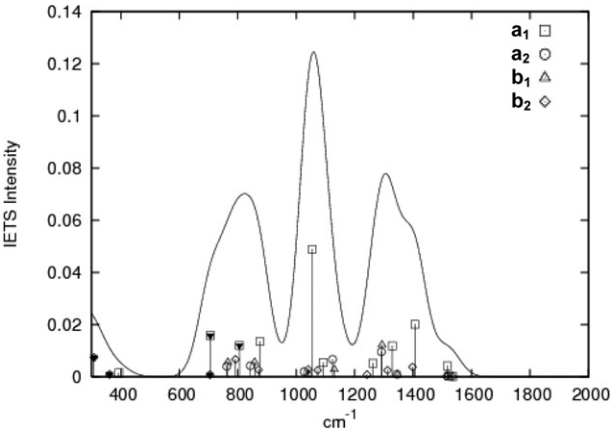

Figure 6. IETS computed spectrum for molecule (**4**).

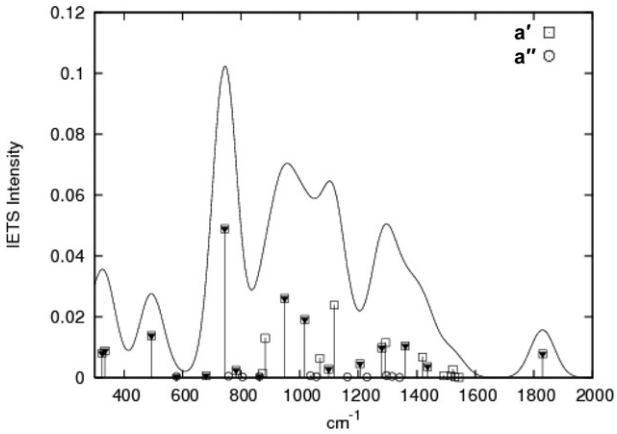

Figure 8. IETS computed spectrum for molecule (**6**).

to a combination of low frequency vibrations and librations of the molecule, only partially reproduced by simulations involving a single molecule. Above 2000 cm^{-1} only the C–H (and N–H) stretching signals are present, which are of lesser significance for the identification of the tunnelling through the functional group. We note incidentally that here, as in previous simulations done with the same approach, the predicted intensity of the CH stretching is smaller than in the experimental measure for reasons the can be related to the orientation of the molecule [67] or the possible compression of the monolayer in the experiment [68].

In figures 3–8 the vertical sticks represent the computed intensity of the normal mode at the corresponding frequency in a $(dI^2/d^2V)/(dI/dV)$ versus V spectrum. The corresponding broadened spectrum is reported in each figure (the chosen broadening of 40 cm^{-1} is smaller than the one experimentally observed to simplify the comparison between figures). The vertical axis shows the intensity computed for the sticks and coincident with the area under the peak. These values are in good agreement with the integrated intensity of the experimental spectrum indicating not only that the physics is described accurately but that the process (where only a small fraction of electrons tunnel inelastically) is well within the limit of validity of the perturbative treatment. Interestingly, if the injection energy is set up close to one of the molecular levels, the computed intensity exceeds unity suggesting a breakdown of the perturbative treatment. In other words, the results of the computation indicate by themselves if the weak coupling limit is appropriate for the system under investigation (a recent experiment investigating in detail the breakdown of the weak coupling limit [69] was published by Yu *et al* [70])

To further simplify the comparison between the series of spectra, in figures 3–8 we labelled (with black triangles) the peaks corresponding to normal modes with the greater contribution from the C, O, N, or S atoms of the central functional group of the molecule (except for molecule **(1)** where we labelled the modes with the greatest contribution from the central carbon atom for comparison). In practice, we ranked the contributions of all normal modes from the largest to the lowest absolute value of the displacement vector of the atoms in the functional group. Therefore, we labelled the peaks if they were in the top 8 of the list (for **(1)**, **(2)**, **(3)**, **(4)**), or in the top 16 of the list (for **(5)**), or in the top 24 (for **(6)**); the three different criteria are justified by the fact that there are from 1 to 3 'heavy' atoms in the functional groups.

The spectrum of the alkane dithiolate has been largely discussed in literature and it is reported here for comparison (figure 3). The experiment shows three main features that are attributed to the C–S stretching (735 cm^{-1} in the unscaled spectrum), to C–C stretching (1010–1090 cm^{-1}) and to the

Table 1. List of the main contributions to the IET spectra of **(1)**.

N	Freq. (cm^{-1})	$1000^{*}W_{\alpha}/g(E_F)$	Sym	Description
1	40.4	34.2	b_1	
2	48.1	10.9	a_1	
3	55.1	2.2	a_2	
4	99.5	21.2	a_2	
5	111.9	1.1	b_1	
7	158.3	2.7	b_1	
8	159.1	0.9	a_2	
9	179.4	11.8	a_1	
10	196.9	1.4	b_1	
11	199.3	2.7	a_2	
12	275.0	5.1	a_1	
13	319.5	0.8	b_2	
15	458.2	11.2	a_1	C–C–C bend
16	735.7	31.9	a_1	C–S stretch
19	752.2	0.8	a_2	
20	775.6	2.1	b_1	
23	875.7	15.3	a_1	C–C–S asym stretch
26	1018.1	18.5	a_1	C–C–C sym stretch
27	1024.3	1.0	b_2	
28	1064.9	28.0	a_1	C–C stretch
30	1077.0	1.8	b_2	
32	1112.6	1.8	a_2	
33	1125.1	0.9	a_1	
35	1244.8	1.0	b_1	
36	1273.3	10.5	a_1	CH_2 wag
41	1356.4	0.9	a_2	
42	1356.7	15.5	a_1	CH_2 wag
44	1397.7	1.8	b_2	
45	1421.4	5.0	a_1	
47	1515.0	1.8	a_1	
51	1526.1	1.1	a_1	
53	1545.4	0.7	a_1	
57	3018.7	1.1	a_1	
58	3027.4	0.7	a_1	

Table 2. List of the main contributions to the IET spectra of **(2)**.

N	Freq. (cm^{-1})	$1000^{*}W_{\alpha}/g(E_F)$	Sym	Description
1	34.1	29.4	b_1	
2	47.0	3.6	a_2	
3	49.7	5.5	a_1	
4	94.0	15.0	a_2	
5	101.7	0.8	b_1	
6	139.6	0.7	b_2	
8	155.1	3.8	b_1	
9	192.4	9.9	a_1	
10	195.1	1.5	b_1	
11	195.5	1.2	a_2	
12	280.7	4.7	a_1	
15	482.0	3.1	a_1	C–O–C bend
16	738.9	28.2	a_1	C–S stretch
17	751.5	0.6	b_2	
19	775.1	0.9	b_1	
23	883.4	12.9	a_1	C–C–S asym stretch
24	1019.6	9.7	a_1	C–O–C sym stretch
25	1057.3	1.6	b_2	
26	1071.4	17.7	a_1	C–C stretch
27	1073.6	1.4	a_2	
29	1090.8	0.8	b_2	
30	1133.6	0.7	a_1	
31	1167.4	0.8	b_2	
34	1271.1	0.7	b_2	
35	1279.6	8.5	a_1	CH_2 wag
36	1307.7	1.1	a_2	
37	1311.3	1.6	b_1	
39	1334.0	0.7	b_1	
40	1365.6	2.0	b_2	
41	1376.8	16.7	a_1	CH_2 wag
43	1476.5	0.7	a_1	
44	1519.8	0.6	b_2	
45	1520.2	1.7	a_1	
49	1567.8	1.1	a_1	

CH_2 wagging (1260–1360 cm^{-1}). The signal at 460 cm^{-1}, usually covered by the tail of the ZBF, is due to the central C–C–C bending motion. The computed spectrum indicates an important contribute of the 875 cm^{-1} mode, not resolved experimentally and due to an asymmetric stretching of the C–C–S group. The spectra of **(2)** and **(3)** (figures 4 and 5) are very similar to that of **(1)**. The signal at 1018 cm^{-1} that in **(1)** is due to the C–C–C central stretching mode, is due to the C–O–C stretching mode (1020 cm^{-1}) in **(2)** and to the C–N–C stretching mode (1035 cm^{-1}) in **(3)**. The signal due to the bending motion of the three central atoms (460–480 cm^{-1}) appears also in **(2)** and **(3)** although it is much weaker in the ether where the displacement of the oxygen is larger. From the comparison of these three spectra, it appears to be impossible, even with an enhanced experimental resolution, to discriminate the presence of an ether or amine groups in a linear alkane chain.

Slightly greater differences are displayed instead by the molecule with the thioether group **(4)**. Instead of the C–S stretching signal at ∼735 cm^{-1}, computed for **(1)**–**(2)**–**(3)**, the presence of the C–S–C group with a very similar vibrational energy causes a redistribution of the frequency and IETS intensity in this region. The symmetric combination of the C–S (terminal) bonds and the C–S–C symmetric stretching are mixed in the modes at 706 and 805 cm^{-1}, with the highest energy vibration displaying a greater contribution of the C–S–C stretching. The bending of the central group C–X–C visible for the first three compounds appears at much lower frequency (255 cm^{-1}) in **(4)** and it is not shown in the figure. The shape of the signal in the 1250–1450 cm^{-1} region is also different in compound **(4)** because of the contribution of non totally symmetrical CH_2 twisting modes discussed in section 4.

A substantially different spectrum is computed for the molecules containing the carbonyl (figure 7) and the ester (figure 8) groups. The characteristic C=O stretching mode is well identifiable in both molecules in a region (1810–30 cm^{-1}) where other vibrational modes are absent. The carbonyl signal has a smaller relative intensity than in IR spectroscopy because, as discussed in [55], the stretching modes that are not along the main tunnelling path (e.g. the side groups) gives a weaker contribution to the IET spectrum. Nevertheless, it is predicted to give a well defined signature that can be used to trace the passage of the electron though that portion of the molecule. In the region 1250–1450 cm^{-1}, a single CH_2 wagging mode at 1343 cm^{-1} dominates the spectrum of **(5)**, while, in the less symmetrical molecule **(6)**, several different modes of the same nature determine a broader feature. Other characteristics features of **(5)** are the central C–C–C symmetric stretching and bending at 888 cm^{-1} and 459 cm^{-1} respectively. **(6)** displays also a characteristic peak at 948 cm^{-1} due to modes

Table 3. List of the main contributions to the IET spectra of **(3)**.

N	Freq. (cm^{-1})	$1000^{*}W_{\alpha}/g(E_F)$	Sym	Description
1	38.2	33.6	a'	
2	48.6	8.1	a'	
3	53.0	3.1	a''	
4	98.4	17.5	a''	
5	107.1	1.7	a'	
7	158.9	3.8	a'	
9	187.5	12.2	a'	
10	199.2	1.7	a'	
11	200.6	1.5	a''	
12	278.8	4.6	a'	
15	471.4	7.4	a'	C–N–C bend
16	734.1	26.3	a'	C–S stretch
18	769.8	0.7	a''	
19	772.1	1.3	a'	
20	806.4	4.3	a'	
23	878.1	12.6	a'	C–C–S asym stretch
24	887.3	3.5	a'	
25	1035.5	11.2	a'	C–N–C sym stretch
26	1041.5	0.9	a''	
27	1063.2	2.0	a''	
28	1068.4	22.8	a'	C–C stretch
30	1084.4	1.4	a''	
31	1139.2	1.0	a'	
32	1158.4	0.9	a''	
34	1249.5	0.8	a'	
36	1281.8	9.7	a'	CH_2 wag
37	1301.1	1.1	a''	
38	1325.9	3.1	a'	
40	1344.3	1.0	a'	
41	1352.3	1.1	a''	
42	1375.7	15.5	a'	CH_2 wag
43	1417.1	0.9	a''	
44	1451.3	1.6	a'	
46	1519.4	1.9	a'	
51	1557.5	1.1	a'	
55	2922.9	0.9	a'	

involving the C–O stretching. The C–C–O bending contributes at 494 cm^{-1} and the O–C=C bending at 335 cm^{-1}. Of course it is also possible to look collectively at these results focusing more on the similarities than on the differences. In this case it can be concluded that, in general, the IET spectra of the functional group will be dominated by two groups of signals (i) stretching signal in the 850–1080 cm^{-1} region and (ii) bending signal in the 250–490 cm^{-1} region both active if involved in the main tunnelling path.

Our results and discussion are certainly more relevant if the characteristic vibrations and intensities can be transferable from molecule to molecule. While it is experimentally well established that vibrational energies of a functional group are very similar across a broad set of molecules, one should notice that the IETS signals are more strongly dependent on the position of the functional group with respect to the electron tunnelling path. As discussed more extensively in [52], the notion that a particular vibration gives a strong IETS signal is valid as long as the chemical environment around that vibration is similar and the group of atoms involved in the vibration is also involved in the main tunnelling path across the molecule. The results presented above are therefore transferable to other molecules if the functional groups are

Table 4. List of the main contributions to the IET spectra of **(4)**.

N	Freq. (cm^{-1})	$1000^{*}W_{\alpha}/g(E_F)$	Sym	Description
1	19.3	184.0	b_1	
2	40.7	5.7	a_2	
3	42.8	3.9	a_1	
4	92.4	133.3	a_2	
5	98.5	49.5	b_1	
6	111.4	69.7	b_1	
7	125.5	4.4	a_2	
8	126.7	5.2	b_2	
9	153.0	8.8	a_1	
10	177.9	12.3	b_1	
11	179.0	9.0	a_2	
12	255.9	7.4	a_1	C–S–C bend
13	308.5	7.4	b_2	
17	706.5	15.7	a_1	C–S stretch combin
18	762.7	4.0	a_2	
19	766.3	5.5	b_1	
20	792.7	6.7	b_2	
21	805.8	12.0	a_1	C–S stretch combin
22	843.7	4.3	a_2	
23	857.7	5.5	b_1	
25	875.2	13.5	a_1	C–C–S asym stretch
29	1055.2	48.9	a_1	C–C stretch
31	1092.0	5.4	a_1	
32	1124.4	6.7	a_2	
35	1262.5	5.2	a_1	
36	1291.5	9.6	a_2	CH_2 twist
37	1293.7	12.2	b_1	CH_2 twist
39	1328.6	11.8	a_1	CH_2 wag
42	1397.9	3.7	b_2	
43	1405.9	20.1	a_1	CH_2 wag
45	1516.9	4.2	a_1	
60	3099.2	4.9	b_1	

Table 5. List of the main contributions to the IET spectra of **(5)**.

N	Freq. (cm^{-1})	$1000^{*}W_{\alpha}/g(E_F)$	Sym	Description
1	23.2	9.6	b_1	
2	29.9	3.3	a_2	
3	51.2	2.0	a_1	
4	79.8	4.4	b_1	
5	86.0	7.3	a_2	
6	117.1	0.5	b_1	
7	117.5	4.1	a_2	
9	181.2	6.2	a_1	
11	197.6	0.9	a_2	
12	268.0	2.6	a_1	
14	323.3	0.7	b_2	
15	460.0	5.0	a_1	C_4–C_5–C_6 bend
16	469.8	0.5	b_1	
19	728.4	13.2	a_1	C–S stretch
25	879.2	13.9	a_1	C–C–S asym stretch
26	888.6	14.5	a_1	C_4–C_5–C_6 sym stretch
29	1064.8	0.5	b_2	
31	1070.7	7.1	a_1	C–C stretch
32	1103.4	1.0	a_1	
36	1265.3	1.9	a_1	
41	1343.7	18.8	a_1	CH_2 wag
44	1415.0	0.5	a_1	
47	1493.0	1.4	a_1	
52	1811.4	5.9	a_1	C=O stretch
56	3024.6	0.4	a_1	
60	3060.4	0.5	a_1	

Table 6. List of the main contributions to the IET spectra of **(6)**.

N	Freq. (cm^{-1})	$1000^{*}W_{\alpha}/g(E_F)$	Sym	Description
1	12.5	12.3	a''	
2	45.0	7.1	a''	
3	53.3	4.7	a''	
4	53.8	2.4	a'	
5	79.5	12.8	a''	
6	105.7	1.5	a''	
9	186.8	23.0	a'	
12	278.9	2.1	a'	
13	325.4	8.0	a'	C–C–S bend
14	335.0	8.8	a'	O=C–O bend
15	494.0	13.8	A'	O–C–O bend
18	743.9	48.9	A'	C–S stretch
20	782.6	2.4	a'	
23	873.4	1.4	a'	
24	882.7	13.0	a'	C–C–S asym stretch
25	948.6	26.0	a'	C–C + C–O stretch
26	1017.6	19.1	a'	C–O stretch
29	1068.8	6.4	a'	
30	1099.1	2.8	a'	
31	1119.1	23.8	a'	C–C stretch
33	1206.1	4.6	a'	
35	1280.7	9.8	a'	CH_2 wag
36	1293.6	11.4	a'	CH_2 wag
40	1360.8	10.4	a'	CH_2 wag
41	1418.6	6.8	a'	
42	1437.0	3.6	a'	
45	1523.5	2.7	a'	
48	1829.7	7.9	a'	C=O stretch
55	3079.6	2.6	a'	
56	3089.2	15.8	a'	

connected to a methylene (–CH_2–) unit on both sides and the electron tunnels though the chain of σ bonds passing through the functional group.

3.2. Symmetry and propensity rules

According to the formal theory described in section 2.1 (and any other available theory for IETS) there are no strict selection rules for this type of spectroscopy, because, after considering all matrix elements that are zero by symmetry, all vibrations may in principle contribute to the spectrum. However, as it is clear from the set of computed and experimental data, there is only a small number of vibrations that display strong IETS activity so that there are probably few propensity rules that is very convenient to explore. In [61] we used two simple observations to derive approximate propensity rules: (i) only for atomic orbital i, j close to the left electrodes Γ^{L}_{ij} is non negligible (and analogously for Γ^{R}_{ij}) and (ii) the Green's function matrix element can be decomposed using the Dyson equation into tunnelling paths. We showed that the vibrations that modulate more strongly the coupling along the main tunnelling path are more IETS intense (they tend to be called 'longitudinal' from the first initial heuristic observations [39, 34]). It is also possible to predict that, if the channel for the tunnelling is predominantly made only by σ orbitals or only by π orbitals (for molecules with a plane of symmetry), the in-plane vibrations dominate the IETS spectrum. Moreover, if there is a symmetry element that interchanges the left and right electrodes (like an inversion centre or a plane parallel to both the electrodes), only normal modes symmetric with respect to this symmetry element will contribute to the IETS. The computations presented here offer the opportunity to verify these predictions on a set of saturated molecules with C_{2v} or C_s symmetry where the main tunnelling channel is made by σ orbitals (it was originally tested on a set of C_{2h} molecules with the main tunnelling channel being made by π orbitals). An alternative proposal of selection rules, leading to slightly different results, was presented in [56, 57].

As illustrated by the tables 1–6 (and graphically by the corresponding figures) the vast majority of the intense absorptions in these molecules derives from totally symmetric vibrations [69]. The few exceptions are the very low frequency modes which, as discussed in [61], allow the injection of the electron into orbital of different symmetry that the dominant one and the signals at 1292 and 1294 cm^{-1} for compound **(4)**. We can argue that the thioether group in **(4)** increases slightly the relative importance of the π channel because of the large contribution to the tunnelling of the sulfur lone pairs. Overall, however, the predominance of totally symmetric modes appears to be a rather robust fact, which can be used for the interpretation of the spectra also in the absence of an explicit simulation.

We conclude this section presenting a comparison of the IETS absorption intensity with the IR and Raman absorption intensities computed with the same quantum chemical method. The comparison with these two spectroscopies has been often used as a guide to understand IETS spectra on the basis of several other analogies among spectroscopic techniques. In the original (on macroscopic surfaces) IETS [71] with quasi-free electrons travelling across the electrodes and in high resolution electron energy loss spectroscopy (HREELS) [72] the molecular dipole–electron interaction determines the inelastic scattering probability and the correlation with IR spectroscopy is appropriate. The correlation IETS/Raman is often attempted because similar samples can be characterized with both techniques [73, 74]. We considered only the totally symmetric vibrations of compound **(2)** and **(6)**, which are both IR and Raman active, and we plot in figures 9(a) and (b) the relative intensities for the three types of spectroscopy. It is evident that not only there is no correlation between IR or Raman intensity and IETS intensity but they seem to obey different propensity rules so that an intense IETS vibration is less likely to be strongly IR or Raman active. Occasional similarities between Raman and IET spectra can be accidental or even due to different vibrations contributing at similar energy to two different spectroscopies, as shown for example in [73].

4. Conclusion

In this paper we studied computationally the characteristic signatures that several common functional groups can leave on a IET spectrum, encouraged by the previous successful comparisons between experimental and theoretical spectra. This study could be used to identify molecules in the junction and to trace the tunnelling paths in systems where more

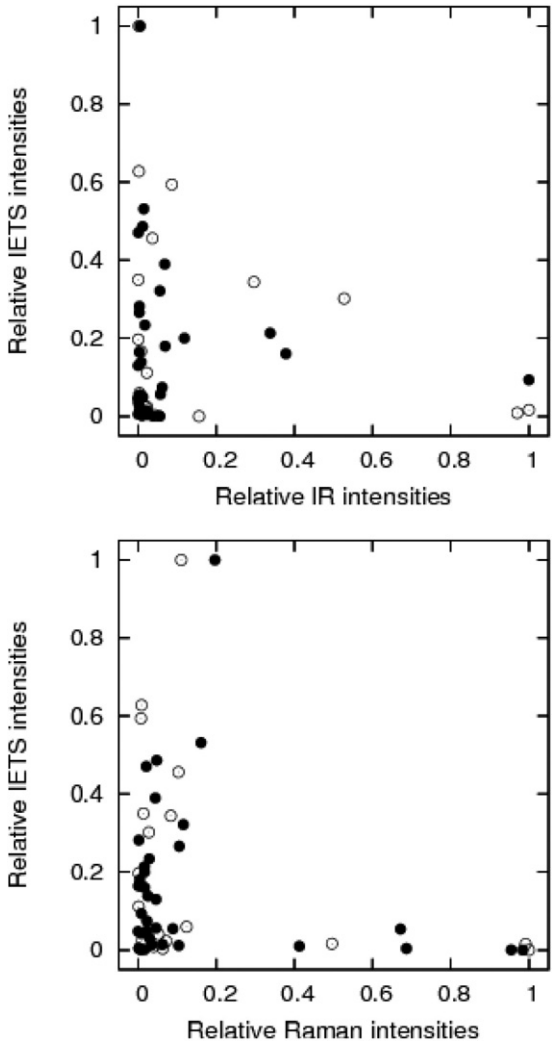

Figure 9. (a) Comparison between relative IR intensity and IETS intensity for the normal modes of molecule **(2)** (empty circles) and **(6)** (full circles). (b) Comparison of the relative Raman and IETS intensities for the same modes. The maximum intensity is set to 1 and only totally symmetric modes are considered.

competing paths are present, following the idea of [52]. We found that the ether, secondary amine and, to a large extent, thioether groups do not introduce important signatures in the spectrum when compared with the reference dithioalkane molecule and we concluded that it will be particularly difficult to establish the presence of these groups from a IETS measurement. On the contrary, the presence of a carbonyl or ester group can be more easily verified thanks to the C=O stretching vibration which is predicted to have a sufficiently high IETS intensity. We also showed that the ester group alters substantially the C–C stretching region of the spectrum making it particularly suitable as a tracer (the passage of the electron through this functional group can be easily recorded by the spectrum). The ability to identify the difference between simple alkanes and functionalized molecules via IETS could be also particular important for the set of experiments where few more 'conductive' molecules are dissolved in an alkane monolayer [21, 75].

This systematic computational study allowed also a further validation of the propensity rules proposed for IETS on the basis of several simple considerations. We verified that totally symmetric vibrations give the largest contribution to IETS also for this set of saturated molecules. This rule is particularly useful for molecules with C_{2v} symmetry but it was heuristically verified also for the molecules with a single symmetry plane perpendicular to the electrode, **(6)**, and parallel to the electrode, **(3)**. It was also verified numerically that there is no correlation between IETS intensities and IR or Raman intensities. It is hoped that this work will stimulate other systematic investigations on similar molecules by theoreticians and experimentalists since it is through a larger number comparisons that we will be able to build a clearer understanding of this important technique.

Acknowledgments

This work was supported by the Royal Society and by EPSRC. The author is grateful to Mark Ratner for his suggestions and constant encouragement.

References

[1] Cuniberti G, Fagas G and Richter K E 2005 *Introducing Molecular Electronics: A Brief Overview* vol 680 (Berlin: Springer)
[2] Nitzan A and Ratner M A 2003 *Science* **300** 1384–9
[3] Joachim C, Gimzewski J K and Aviram A 2000 *Nature* **408** 541–8
[4] Joachim C, Gimzewski J K, Schlittler R R and Chavy C 1995 *Phys. Rev. Lett.* **74** 2102–5
[5] Reed M A, Zhou C, Deshpande M R, Muller C J, Burgin T P, Jones L II and Tour J M 1998 *Annu. New York Acad. Sci.* **852** 133–44
[6] Park J, Pasupathy A N, Goldsmith J I, Chang C, Yaish Y, Petta J R, Rinkoski M, Sethna J P, Abruna H D, McEuen P L and Ralph D C 2002 *Nature* **417** 722–5
[7] Chen F, Hihath J, Huang Z F, Li X L and Tao N J 2007 *Annu. Rev. Phys. Chem.* **58** 535–64
[8] Lindsay S M and Ratner M A 2007 *Adv. Mater.* **19** 23–31
[9] Tersoff J and Hamann D R 1985 *Phys. Rev.* B **31** 805–13
[10] Mujica V, Kemp M, Roitberg A and Ratner M 1996 *J. Chem. Phys.* **104** 7296–305
[11] Kadanoff L P and Baym G 1962 *Quantum Statistical Mechanics. Green's Function Methods in Equilibrium and Nonequilibrium Problems* (Reading, MA: Benjamin)
[12] Datta S 1995 *Electric Transport in Mesoscopic Systems* (Cambridge: Cambridge University Press)
[13] Xue Y, Datta S and Ratner M A 2001 *J. Chem. Phys.* **115** 4292–9
[14] Ke S H, Baranger H U and Yang W T 2005 *J. Chem. Phys.* **123** 114701
[15] Basch H and Ratner M A 2005 *J. Chem. Phys.* **123** 234704
[16] Nakamura H and Yamashita K 2006 *J. Chem. Phys.* **125** 194106
[17] Wang J G and Selloni A 2007 *J. Phys. Chem.* A **111** 12381–5
[18] Galperin M, Ratner M A and Nitzan A 2007 *J. Phys.: Condens. Matter* **19** 103201
[19] Troisi A and Ratner M A 2004 *Nano Lett.* **4** 591–5
[20] Qiu X H, Nazin G V and Ho W 2004 *Phys. Rev. Lett.* **93** 196806
[21] Lewis P A, Inman C E, Yao Y X, Tour J M, Hutchison J E and Weiss P S 2004 *J. Am. Chem. Soc.* **126** 12214–5
[22] Haiss W, Wang C S, Grace I, Batsanov A S, Schiffrin D J, Higgins S J, Bryce M R, Lambert C J and Nichols R J 2006 *Nat. Mater.* **5** 995–1002

[23] Jones D R and Troisi A 2007 *J. Phys. Chem.* C **111** 14567–73
[24] Holstein T 1959 *Ann. Phys., Lpz.* **8** 325
[25] Coropceanu V, Cornil J, da Silva D A, Olivier Y, Silbey R and Bredas J L 2007 *Chem. Rev.* **107** 926–52
[26] Galperin M, Ratner M A and Nitzan A 2005 *Nano Lett.* **5** 125–30
[27] Blum A S, Kushmerick J G, Long D P, Patterson C H, Yang J C, Henderson J C, Yao Y X, Tour J M, Shashidhar R and Ratna B R 2005 *Nat. Mater.* **4** 167–72
[28] Lortscher E, Ciszek J W, Tour J and Riel H 2006 *Small* **2** 973–7
[29] Troisi A and Ratner M A 2006 *Small* **2** 172–81
[30] Galperin M, Ratner M A, Nitzan A and Troisi A 2008 *Science* **319** 1056–62
[31] Jaklevic R C and Lambe J 1966 *Phys. Rev. Lett.* **17** 1139–40
[32] Hipps K W and Mazur U 1993 *J. Phys. Chem.* **97** 7803–14
[33] Stipe B C, Rezaei M A and Ho W 1998 *Science* **280** 1732–5
[34] Kushmerick J G, Lazorcik J, Patterson C H, Shashidhar R, Seferos D S and Bazan G C 2004 *Nano Lett.* **4** 639–42
[35] Wang W Y, Lee T, Kretzschmar I and Reed M A 2004 *Nano Lett.* **4** 643–6
[36] Mingo N and Makoshi K 2000 *Phys. Rev. Lett.* **84** 3694–7
[37] Lorente N, Persson M, Lauhon L J and Ho W 2001 *Phys. Rev. Lett.* **86** 2593–6
[38] Paavilainen S and Persson M 2006 *Phys. Rev.* B **74** 085417
[39] Troisi A, Ratner M A and Nitzan A 2003 *J. Chem. Phys.* **118** 6072–82
[40] Troisi A and Ratner M A 2005 *Phys. Rev.* B **72** 033408
[41] Long D P, Lazorcik J L, Mantooth B A, Moore M H, Ratner M A, Troisi A, Yao Y, Ciszek J W, Tour J M and Shashidhar R 2006 *Nat. Mater.* **5** 901–8
[42] Toroker M C and Peskin U 2007 *J. Chem. Phys.* **127** 154706
[43] Jiang J, Kula M, Lu W and Luo Y 2005 *Nano Lett.* **5** 1551–5
[44] Kula M, Jiang J and Luo Y 2006 *Nano Lett.* **6** 1693–8
[45] Paulsson M, Frederiksen T and Brandbyge M 2006 *Nano Lett.* **6** 258–62
[46] Frederiksen T, Paulsson M, Brandbyge M and Jauho A P 2007 *Phys. Rev.* B **75** 205413
[47] Solomon G C, Gagliardi A, Pecchia A, Frauenheim T, Di Carlo A, Reimers J R and Hush N S 2006 *J. Chem. Phys.* **124** 094704
[48] Frauenheim T, Seifert G, Elstner M, Niehaus T, Kohler C, Amkreutz M, Sternberg M, Hajnal Z, Di Carlo A and Suhai S 2002 *J. Phys.: Condens. Matter* **14** 3015–47
[49] Reimers J R, Solomon G C, Gagliardi A, Bilic A, Hush N S, Frauenheim T, Di Carlo A and Pecchia A 2007 *J. Phys. Chem.* A **111** 5692–702
[50] Soler J M, Artacho E, Gale J D, Garcia A, Junquera J, Ordejon P and Sanchez-Portal D 2002 *J. Phys.: Condens. Matter* **14** 2745–79
[51] Teobaldi G, Penalba M, Armau A, Lorente N and Hofer W 2007 *Phys. Rev.* B **76** 235407
[52] Troisi A, Beebe J M, Picraux L B, van Zee R D, Stewart D R, Ratner M A and Kushmerick J G 2007 *Proc. Natl Acad. Sci. USA* **104** 14255–9
[53] Onuchic J N, Beratan D N, Winkler J R and Gray H B 1992 *Annu. Rev. Biophys. Biomol. Struct.* **21** 349–77
[54] Jones M L, Kurnikov I V and Beratan D N 2002 *J. Phys. Chem.* A **106** 2002–6
[55] Troisi A and Ratner M A 2006 *Nano Lett.* **6** 1784–8
[56] Solomon G C, Gagliardi A, Pecchia A, Frauenheim T, Di Carlo A, Reimers J R and Hush N S 2006 *J. Chem. Phys.* **125** 184702
[57] Gagliardi A, Solomon G C, Pecchia A, Frauenheim T, Di Carlo A, Hush N S and Reimers J R 2007 *Phys. Rev.* B **75** 174306
[58] Meir Y and Wingreen N S 1992 *Phys. Rev. Lett.* **68** 2512–5
[59] Nitzan A 2004 *Nano Lett.* **4** 1605–11
[60] Galperin M, Ratner M A and Nitzan A 2004 *J. Chem. Phys.* **121** 11965–79
[61] Troisi A and Ratner M A 2006 *J. Chem. Phys.* **125** 214709
[62] Huang J and Kertesz M 2004 *Chem. Phys. Lett.* **390** 110–5
[63] Rauhut G and Pulay J 1995 *J. Phys. Chem.* **99** 3093
[64] Silverstein R, Webster F and Kiemle D 2005 *Spectrometric Identification of Organic Compounds* 7th edn (New York: Wiley)
[65] Love J C, Estroff L A, Kriebel J K, Nuzzo R G and Whitesides G M 2005 *Chem. Rev.* **105** 1103–69
[66] Claypool C L, Faglioni F, Goddard W A, Gray H B, Lewis N S and Marcus R A 1997 *J. Phys. Chem.* B **101** 5978–95
[67] Troisi A and Ratner M A 2007 *Phys. Chem. Chem. Phys.* **9** 2421–7
[68] Beebe J M, Moore H J, Lee T R and Kushmerick J G 2007 *Nano Lett.* **7** 1364–8
[69] Galperin M, Nitzan A and Ratner M A 2006 *Phys. Rev.* B **73** 045314
[70] Yu L H, Zangmeister C D and Kushmerick J G 2007 *Phys. Rev. Lett.* **98** 206803
[71] Wolf E L 1985 *Principles of Electron Tunneling Spectroscopy* (New York: Oxford University Press)
[72] Ibach H and Mills D 1982 *Electron Energy Loss Spectroscopy and Surface Vibrations* (New York: Academic)
[73] Long D P and Troisi A 2007 *J. Am. Chem. Soc.* **129** 15303–10
[74] Zhao Y, Segarra W, Shi Q and Wei A 2005 *J. Am. Chem. Soc.* **127** 7328–9
[75] Donhauser Z J, Mantooth B A, Kelly K F, Bumm L A, Monnell J D, Stapleton J J, Price D W Jr, Rawlett A M, Allara D L, Tour J M and Weiss P S 2001 *Science* **292** 2303–7